Nonlinear Normal Modes, Modal Interactions and Isolated Resonance Curves

R.J. Kuether[1], L. Renson[2], T. Detroux[2], C. Grappasonni[2], G. Kerschen[2], M.S. Allen[1]

[1] Department of Engineering Physics,
University of Wisconsin-Madison,
Madison, WI 53706.

[2]Space Structures and Systems Laboratory,
Department of Aerospace and Mechanical Engineering,
University of Liège, Liège, Belgium.

Corresponding author: L. Renson
Email: l.renson@ulg.ac.be, phone: +32 4 3664854.

Abstract

The objective of the present study is to investigate isolated resonance curves in the neighborhood of nonlinear normal mode (NNM) interactions. Isolated resonance curves are separate from the nonlinear forced response that is typically computed by initiating a continuation algorithm at a low energy, linear solution, so they can easily be missed causing the resonant response to be under-predicted. This work explores the connection between these isolated resonances and the nonlinear normal modes of the undamped system and adapts an energy balance criterion to connect the two. This provides new insights into the occurrence of isolated resonances as well as a method to find an initial guess that can be used to compute the isolated resonance curve using numerical continuation. These concepts are illustrated on a finite element model of a cantilever beam with a nonlinear spring at its tip. The nonlinear modes and nonlinear forced response are shown to explain jumps in both frequency and amplitude in the beam's response to a swept sinusoidal excitation. The jumps are found to be the result of a modal interaction that creates an isolated resonance curve that merges with the main resonance branch as the excitation force increases causing the frequency jump. Excellent insight into the observed dynamics is provided with the NNM theory, which supports that NNMs can also be a useful tool for predicting isolated resonance curves and other behavior in the damped, forced response.

Keywords: nonlinear normal modes; modal interaction; nonlinear forced response; isolated resonance curves; fold bifurcations.

1 Introduction

Nonlinearity is important in many structural dynamic applications that are of interest to engineers, for example in structures with bolted interfaces [1], machinery with rubber isolation mounts, microsystems subjected to thermal, magnetic or friction forces [2], and biomechanical systems [3]. In other cases the baseline structure is linear, but its performance can be enhanced by adding or engineering certain types of nonlinearities [4, 5]. However, nonlinear dynamics is a rich and complicated field and so engineers tend instead to ignore nonlinearity or to seek a linear model that approximates the system at the forcing level of interest [6].

Vibration modes form the foundation of our understanding of linear dynamic systems, and influence efforts related to testing, modeling, validating and controller design. Rosenberg [7] extended modal analysis to nonlinear systems in the 1960's, coining the phrase nonlinear normal mode (NNM). The area received new attention in the 1990's [8–10] and now it is clear that NNMs can be used to obtain a wealth of insight into the response of a nonlinear system [9, 11]. For example, NNMs have been used to explain internally resonant and non-resonant motions of structures [12], to design a nonlinear vibration absorber (also called a nonlinear energy sink) [4], to create or validate a reduced order model for a system [13], and to explain changes in the oscillation frequency and the deformation shape of the free and forced response of a structure [11].

In recent years important progress has been made in the numerical calculation of undamped [14–17] and damped NNMs [18, 19]. These new algorithms have been used to compute the nonlinear modes of a geometrically nonlinear finite element model of a component from a diesel exhaust system, a full-scale aircraft, a bladed disk from a turbine and a strongly nonlinear satellite in [15, 20–22], respectively. A framework for experimental identification of NNMs was recently presented in [23] and validated on an academic structure [24]. More recent works have begun to use this framework on more complicated structures [25, 26].

One fundamental property of undamped NNMs is the fact that they can be realized when a harmonic forcing function cancels the damping force in the damped system [23]. As a result, they form the backbone of the nonlinear forced response (NLFR) curves [10, 11, 27] and hence they approximate the oscillation frequency and deformation shape that are exhibited at resonance, when a structure is at the greatest risk of failure. The relationship between the NLFR and the NNM backbone is simple for mild nonlinearities, but most realistic systems exhibit complicated NNMs with many interactions between the various modes leading to internally resonant branches. Many works have explored interactions between nonlinear modes with commensurate linear frequencies, e.g., when a pair of the linearized natural frequencies of the system have an integer ratio [28–30]. Some of them have even exploited these modal interactions for optimal design [31]. In contrast, only a few have considered the case that is of interest in this work where the modal interactions occur between pairs of modes whose linear frequencies are not integer related. The investigation of such interactions requires one to resort to computational methods, which is another specific aspect of this study.

This work explores the relationships between these interacting NNMs and the forced response of the nonlinear system, especially for the case in which the forced response shows an isolated resonance curve (IRC). Specifically, we show that the interactions between NNMs are responsible for the IRCs in the forced response. We note that the paper [32] discusses the relationships between bifurcations of backbone curves and IRCs; it is therefore the ideal companion of the present study. These detached families of solutions are frequently not detected because they do not emerge naturally from the fundamental response when numerical continuation is used. They can lie outside or inside the main resonance curve [33,34], with the former case typically being more important because one is likely to underestimate the response of the nonlinear system [35,36]. Isolated resonances may also go undetected during laboratory experiments when stepped/swept sine testing is employed.

The paper is organized as follows. Section 2 reviews the methodology used to compute the periodic motions of the undamped and damped form of the nonlinear equations of motion, along with a phase resonance condition extended to nonlinear systems. An adaptation of the energy balance procedure presented by Neild et al. [37, 38], which can be used to estimate the forcing amplitude required to isolate the NNM is also presented in Section 2, drawing a direct connection between the damped and undamped periodic solutions. The nonlinear modes of a linear cantilever beam with a cubic nonlinear spring attached at the beam tip are computed in Section 3, showing that modal interactions can still occur even when the underlying linear modes have non-commensurate frequencies. The NLFR of this system is presented in Section 4, where an IRC is discovered near one of the modal interactions of the underlying undamped NNMs. Section 5 explores the effect of damping on the IRCs by tracking the fold bifurcations in the NLFR as the level of damping changes. The conclusions of the present study are presented in Section 6.

2 Periodic Solutions of a Nonlinear System

2.1 Periodic Motions of an Undamped System: Nonlinear Normal Modes

The N-degree-of-freedom (DOF) equations of motion (EOM) for a nonlinear finite element model generally can be written as

$$\mathbf{M}\ddot{\mathbf{x}} + \mathbf{C}\dot{\mathbf{x}} + \mathbf{K}\mathbf{x} + \mathbf{f}_{NL}(\mathbf{x}) = \mathbf{f}(t) \tag{1}$$

The $N \times N$ matrices $\mathbf{M}$, $\mathbf{C}$, and $\mathbf{K}$ respectively represent the linear mass, damping and stiffness matrices commonly used for linear models. The displacement, velocity and acceleration are represented with the $N \times 1$ vectors $\mathbf{x}$, $\dot{\mathbf{x}}$, and $\ddot{\mathbf{x}}$, and the external loads are applied through the $N \times 1$ force vector $\mathbf{f}(t)$. The $N \times 1$ nonlinear restoring force vector, $\mathbf{f}_{NL}(\mathbf{x})$, accounts for the nonlinearity in the physical system. In this work we only consider the case where the nonlinear restoring force depends on displacement. This assumption can be restricting since many interesting applications have velocity dependent

nonlinearity (e.g. jointed structures with nonlinear damping [39]), however these are not considered because of the developments that follow in this section.

The undamped NNM definition used in this work comes from the works of Lee [40] and Kerschen et al. [11]. They defined an NNM as *a not necessarily synchronous periodic motions of the conservative equations of motion*. By this definition, the periodic motions that occur when two or more modes interact are still considered NNMs since they relaxed the restriction of synchronous motion defined originally by Rosenberg [7]. Many new features emerge with this definition of a vibration mode that cannot be described with linear modal analysis, such as frequency-energy dependence, bifurcations, localization, and modal interactions. Typically, the NNMs are represented on the frequency-energy plane, as shown later in Sections 3 and 4, showing how the fundamental frequency of the periodic motion changes as the energy of the system (which is conserved over the period of the response) evolves.

These nonlinear vibration modes require an alternate computational method due to the nonlinear terms in the EOM. In general, a periodic solution is sought, which must always satisfy the condition

$$\mathbf{z}(t+T) = \mathbf{z}(t), \quad \forall\, t \tag{2}$$

The state of the system $\mathbf{z} = [\mathbf{x}^{\mathrm{T}} \quad \dot{\mathbf{x}}^{\mathrm{T}}]^{\mathrm{T}}$, where $(\cdot)^{\mathrm{T}}$ represents the transpose operator, relates to the displacement and velocity of the undamped form of Eq. (1). A variety of methods exist to find the periodic solutions (or NNMs) for the undamped EOM, such as perturbation techniques [4] and the harmonic balance approach [41]. In this work we employ the shooting technique [42] combined with numerical integration and a Newton-Raphson scheme to iteratively find the periodic solutions that satisfy Eq. (2). A shooting function is defined as the difference between the initial state and the state of the system after some period of integration, T. Mathematically, the shooting function is written as,

$$\mathbf{H}(\mathbf{z}_0, T) = \mathbf{z}(\mathbf{z}_0, T) - \mathbf{z}_0 = \mathbf{0} \tag{3}$$

Given an initial state, $\mathbf{z}_0$, and a minimum oscillation period, T, that satisfy the periodicity condition in Eq. (3) to some numerical tolerance, the resulting periodic motion over that period is subsequently defined as the NNM.

When the shooting technique is combined with numerical continuation (as done in [15,17]), a continuous branch of NNMs is computed, showing the evolution of the periodic motions as the energy changes. Numerical continuation requires that a known solution exist in order to trace out a branch of solutions, making the linear normal modes at low energy an excellent starting point.

2.2 Periodic Motions of a Damped System: Nonlinear Forced Response

The damped system includes the linear damping and external forces in the EOM, exactly as given in Eq. (1). In this work, the periodic motions refer to the steady state motion

in response to a monoharmonic excitation force, which is defined as

$$\mathbf{f}(t) = \mathrm{Re}\left(\mathbf{F}e^{i\omega t}\right) \tag{4}$$

The complex amplitude vector $\mathbf{F}$ is arbitrarily applied at any of the systems DOF. The steady state response to the force in Eq. (4) at each forcing frequency, ω, is referred to as the nonlinear forced response (NLFR). An approximation to the true NLFR can be found using the harmonic balance method [43], which creates a set of nonlinear algebraic relations between the Fourier coefficients of the response and harmonic force coefficients. The truncation of harmonics in the response makes this approach inherently approximate, although it has been used successfully in many applications such as [44].

In this work we instead employ a solution that is similar to that used to find NNMs above, namely, shooting combined with numerical continuation in order to find the NLFR over a range of forcing frequencies. The shooting function is only slightly different from the one used to find the NNMs in Eq. (3), as

$$\mathbf{H}(\mathbf{z}_0, \omega, T) = \mathbf{z}(\mathbf{z}_0, \omega, T) - \mathbf{z}_0 = \mathbf{0} \tag{5}$$

This function evaluates the difference of the forced response at time T due to a forcing frequency ω and a set of initial conditions, $\mathbf{z}_0$. The shooting technique with numerical integration and a Newton-Raphson procedure is again combined with numerical continuation to find a continuous branch of solutions for a fixed forcing amplitude, $\mathbf{F}$. The continuation algorithm initially requires a known solution, therefore a low-energy, steady state response of the linearized system away from resonance generally offers a good starting point since it can be predicted analytically from the frequency response function. Unlike the linear case, the NLFR does not scale linearly with forcing amplitude, so a new NLFR branch must be computed for each amplitude of interest. The NLFR reveals new phenomena that cannot be observed with linear theory, such as frequency-energy dependence, subharmonic and superharmonic resonances, coexisting solutions, and stable/unstable periodic motions.

The objective of this work is to study IRCs, which cannot be arrived at by continuing from the linear response at low energy. The next two subsections discuss the connection between the NNMs and the NLFR. This leads to several insights and the important finding that the NNMs can be used to obtain a solution from which continuation can be initiated to compute an IRC.

2.3 Resonance of a Nonlinear System: Phase Quadrature

This section reviews the derivation of the force appropriation technique that was originally discussed in [23], in order to highlight the connections between the NLFR and the NNMs. The damped system can be made to respond in a single NNM motion if a multi-point, multi-harmonic excitation is applied to the system in Eq. (1). Specifically, this force is given as

$$\mathbf{f}(t) = \sum_{k=1}^{\infty} \mathrm{Re}\left(\mathbf{F}_k e^{ik\omega t}\right) \tag{6}$$

The fully populated $N \times 1$ vector $\mathbf{F}_k$ corresponds to the complex amplitude of the force for the k^{th} harmonic frequency. In response to this force, a periodic motion is realized resulting in a complex Fourier series representation of the response and nonlinear restoring force as

$$\mathbf{x}(t) = \sum_{k=1}^{\infty} \text{Re}\left(\mathbf{X}_k e^{ik\omega t}\right) \tag{7}$$

$$\mathbf{f}_{NL}(t) = \sum_{k=1}^{\infty} \text{Re}\left(\mathbf{F}_{NL,k} e^{ik\omega t}\right) \tag{8}$$

The $N \times 1$ vectors $\mathbf{X}_k$ and $\mathbf{F}_{NL,k}$ are the complex amplitudes for the k^{th} harmonic of the response and nonlinear restoring force, respectively. Note that the nonlinear force depends on the actual response, or the sum of all of the harmonics $\mathbf{X}_k$, so the k^{th} harmonic of the force, $\mathbf{F}_{NL,k}$, actually depends on all harmonics of the response, $\mathbf{X}_k$, for $k = 1, ..., \infty$. By substituting Eqs. (6)-(8) and the respective time derivatives of displacement into Eq. (1), each harmonic can be balanced to give the following two relations

$$-k^2\omega^2\mathbf{M}\mathbf{X}_k + \mathbf{K}\mathbf{X}_k + \mathbf{F}_{NL,k} = 0 \tag{9}$$

$$ik\omega\mathbf{C}\mathbf{X}_k = \mathbf{F}_k \tag{10}$$

These equations reveal an important relationship between the forced response and the NNMs of the system. That is, if all harmonics of the force exactly cancel out the harmonics of the damping forces given by Eq. (10), then the periodic response will exactly satisfy the undamped EOM, as shown by Eq. (9), which by definition is an NNM. In an experimental context the NNM is not known, so instead the objective is to adjust the forcing in order to experimentally identify an NNM. In this case, one does not know what multi-harmonic force to use, but a harmonic force near resonance can be applied and the higher harmonics adjusted until each harmonic of the displacement is 90 degrees out of phase with respect to the force harmonics. This phase lag quadrature condition can be used to indicate when an NNM motion has been isolated from the NLFR.

Of course, in practice it is unlikely that the forcing of interest will exactly cancel damping as outlined above, because this requires that the force be distributed in space and that it be comprised of many harmonics. A few studies [23–26, 46] have shown that an accurate approximation to the NNM can be obtained by a much simpler force that excites resonance. For example, Peeters et al. [23,24] explored whether a single-point, monoharmonic excitation could approximately isolate an NNM, and found good results in simulations and experiment with a lightly damped beam. In their efforts it was helpful to define a multi-harmonic mode indicator function (MIF) which indicates when the 90 degrees phase lag condition has been obtained. When a single-point sinusoidal force is applied to the nonlinear structure, which is the case considered herein, the MIF is defined as follows

$$\Delta_1 = \frac{\text{Re}(\mathbf{X}_1)^* \text{Re}(\mathbf{X}_1)}{\mathbf{X}_1^* \mathbf{X}_1} \tag{11}$$

where the operator $(\cdot)^*$ represents the complex conjugate transpose. Using the complex amplitude of the fundamental harmonic, $\mathbf{X}_1$, of the computed NLFR, the MIF in Eq. (11) indicates that resonance occurs when Δ_1 is equal to one.

2.4 Force Required to Obtain NNM Motion

The relationship between backbone curves and the forced response was also studied using an energy balancing technique in [37,38]. Based on the second-order normal form theory, the analytical developments hold for weakly nonlinear regimes of motion. This technique is slightly revisited herein by employing a numerical viewpoint, which allows one to consider more strongly nonlinear regimes.

Let us first consider a linear system. As shown in [47], if the system is oscillating in a linear normal mode denoted as $\mathbf{x}(t)$, then the damping forces instantaneously exert a distributed force $\mathbf{C}\dot{\mathbf{x}}(\mathbf{t})$ and the power dissipated at any instant is

$$P_{diss} = \dot{\mathbf{x}}(t)^{\mathrm{T}}\mathbf{C}\dot{\mathbf{x}}(\mathbf{t}) \tag{12}$$

and the total energy dissipated over one cycle is

$$E_{diss/cyc} = \int_0^T P_{diss}\, dt \tag{13}$$

Similarly, an arbitrary forcing function $\mathbf{f}(t)$ inputs energy into the system as

$$E_{in/cyc} = \int_0^T \dot{\mathbf{x}}(t)^{\mathrm{T}}\mathbf{f}(t)\, dt \tag{14}$$

At resonance, the energy dissipated by the damping forces must match the total energy input to the system over the period T. The balance is enforced by setting $E_{diss/cyc} = E_{in/cyc}$ [47]. For a single-point, monoharmonic force with complex amplitude $A + i0$, the scaling on A can be computed by satisfying

$$A\int_0^T \dot{\mathbf{x}}(t)^{\mathrm{T}}\left(\mathbf{e}_n e^{i\omega t}\right)\, dt = \int_0^T \dot{\mathbf{x}}(t)^{\mathrm{T}}\mathbf{C}\dot{\mathbf{x}}(\mathbf{t})\, dt \tag{15}$$

where $\mathbf{e}_n$ is a vector of zeros with a value of one at the location n, which is the point at which the force is applied. This energy balance criterion is a useful result, because it enables the practitioner to establish formally the direct link from the computed linear normal modes, i.e., the periodic motions of the undamped, unforced system, to the resonant response of the damped forced system.

The energy balance, $E_{diss/cyc} = E_{in/cyc}$, also holds for nonlinear systems. So, if both the NNMs $\mathbf{x}(t)$ and the damping $\mathbf{C}$ in the system are known, Eq. (15) can be readily used to estimate the forcing amplitude A that would excite the system at resonance with associated motion $\mathbf{x}(t)$. While it is common practice to excite a system using a monoharmonic force, one should note that higher harmonics might be necessary to achieve a reasonable approximation to the NNM motion, especially near internal resonances, so any calculations based on Eq. (15) should be regarded as approximate.

As in [37, 38], the energy balance criterion will prove useful for computing the forced resonant response in correspondence to the backbone curve. Sections 4 and 5 will show that it can also be used in conjunction with the NNM to find the forcing amplitude at which IRCs are created and to compute the corresponding forced response.

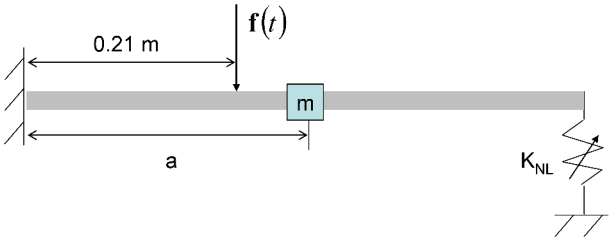

Figure 1: Schematic of a cantilever beam with a cubic nonlinear spring attached to the beam tip and a modifying lumped mass.

3 Numerical Case Study: Nonlinear Normal Modes of a Cantilever Beam

In the present and next sections, a model of a cantilevered beam with a cubic nonlinear spring attached at the beam tip is used to investigate the connection between undamped NNMs and the damped NLFR.

A schematic of the FEA model is shown in Fig. 1, which is similar to the one studied in [17]. A lumped mass of 0.5 kg was added $a = 0.31$ m from the fixed end. The addition of the mass lowered the second natural frequency most, while having a minimal effect on the first mode. This shifted the location of the 3:1 modal interaction with NNM 2 on the first NNM branch (as seen later in Fig. 2(a)). A linear finite element model of the planar beam was created in Abaqus using 20 B31 Euler-Bernoulli beam elements, giving it a total of 60 DOF, where each node had x and y displacement, and z rotation. The beam was 0.7 m in length, with a width and thickness of 0.014 m, and was constructed of structural steel with a Young's modulus of 205 GPa and a density of 7800 kg/m^3. The cubic nonlinear spring had a coefficient of $K_{NL} = 6\,10^9 N/m^3$, and was attached at the beam tip affecting only the transverse direction. The first four NNMs of the cantilever beam were computed using the shooting and pseudo-arclength continuation algorithm, and the frequency-energy plots (FEPs) of these are shown in Fig. 2, where the black line represents the stable periodic solutions and the red dots are unstable. Each NNM branch initiated at low energy at a linear mode. As the response amplitude in each nonlinear mode increased, the continuation algorithm traced the family of NNMs forming a continuous branch of solutions. These FEPs have two distinct features, namely a backbone, and tongues that emanate from the backbone. The backbone of NNM 1 in Fig. 2(a) shows an increase in fundamental frequency as the energy in the periodic solutions increased revealing that the nonlinear spring has a stiffening effect on this mode. Each of the first four NNMs showed this stiffening behavior, but the energy level at which the nonlinearity began to affect the frequency and deformation varied for each. The tongues that emerged from the backbones along each NNM are referred as modal interactions, or internal resonances, and occur when two or more NNMs interact. The response of the NNM at locations on these tongues showed a strong, multi-harmonic response at an integer frequency ratio of the interacting nonlinear mode.

Figure 2(a) displays a detailed view of the FEP of NNM 1, where the dashed, colored

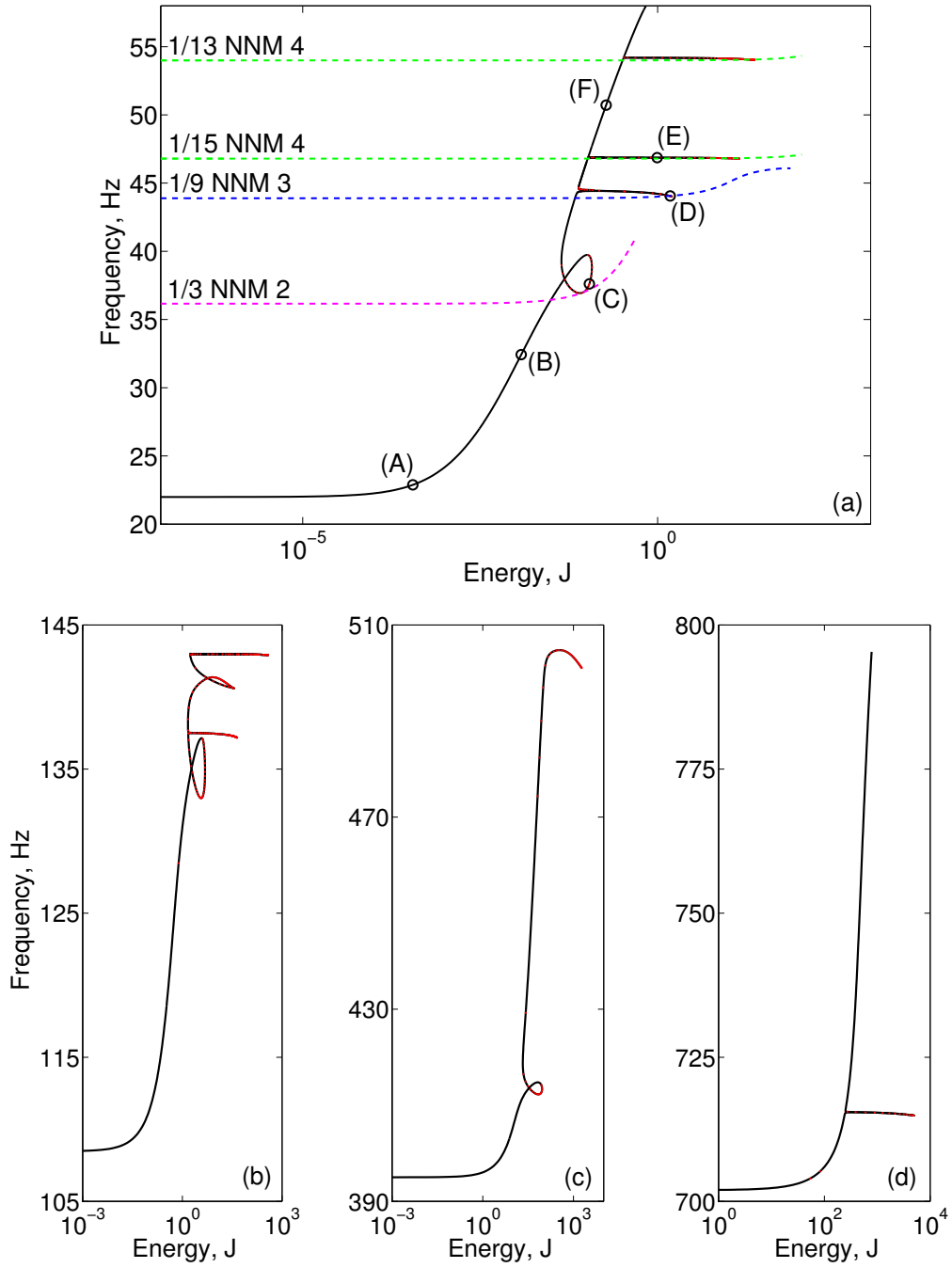

Figure 2: The nonlinear normal modes of the nonlinear beam: (a) NNM 1, (b) NNM 2, (c) NNM 3, and (d) NNM 4. Solid black represents a stable solution, and dotted red represents an unstable solution. The detailed view of NNM 1 shows the crossing of higher order NNMs in dashed lines at fractions of their fundamental frequency. The time histories of solutions (A)-(F) along NNM 1 are shown in Fig. 3.

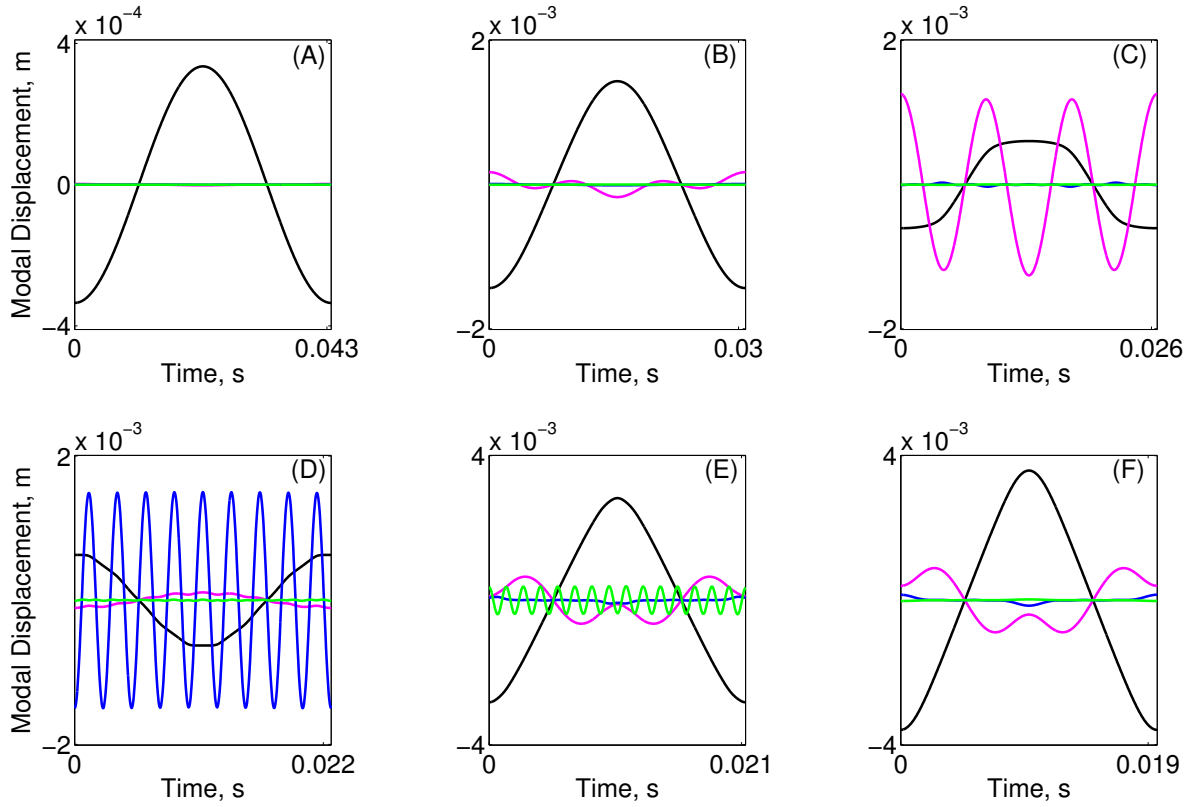

Figure 3: Time histories of a NNM motion at discrete locations of the NNM 1 FEP in Fig. 2(a). The color code for each modal coordinate is (black) mode 1, (magenta) mode 2, (blue) mode 3 and (green) mode 4.

lines represent the frequency-energy behavior of the higher order NNMs after dividing the frequency by various integers. By shifting these NNMs down the frequency axis, it was possible to observe the location where the backbones of higher modes intersect with the NNM 1 backbone and cause a modal interaction to occur. Considering the modal interaction at approximately 37 Hz, which has the appearance of the Greek letter α and will hereafter be referred to as an α-tongue, the 1/3rd frequency branch of the NNM 2 branch intersects the backbone of NNM 1. This causes NNM 1 to bifurcate and create a 3:1 internal resonance tongue that has solutions where NNM 1 and 2 interact. The other three modal interactions along NNM 1 were a 9:1 interaction with NNM 3 near 44 Hz, a 15:1 interaction with NNM 4 near 47 Hz, and a 13:1 interaction with NNM 4 near 54 Hz. These modal interactions occurred even though the underlying linear modes did not have commensurate frequencies, meaning the frequency-energy dependence caused the NNMs to have commensurate frequencies; this result is not often discussed in the literature. It is also important to note that NNM 1 in Fig. 2(a) was almost certainly incomplete, because in reality many more tongues could emanate from the backbone as the frequency is equal to many other integer fractions of higher NNMs. These additional tongues must have been missed by the continuation algorithm. In principle they could be found using a smaller stepsize but this becomes time consuming and was not pursued.

The response at each of the points (A)-(F) along NNM 1 in Fig. 2(a) is presented in Fig. 3, where each physical response was projected onto the unit displacement normalized modes and plotted over one period. This normalization of the mode shapes allows the modal coordinates to be presented in units of meters. The time histories in Figs. 3(A,B,F) correspond to locations along the backbone of NNM 1. At low energy, the response in Fig. 3(A) was dominated by the first linear mode (black line), while other modes were quiescent. This was expected since at low energies the NNMs converge to the underlying linearized modes of the system. At higher energies, the responses in Figs. 3(B,F) showed that other modal coordinates contributed to the overall response (i.e. mode 2 and mode 3 in particular). The nonlinearity essentially coupled all of the underlying linear modes at higher energy levels, causing the frequency and deformation shapes of the periodic motions to change with amplitude.

The three plots in Figs. 3(C,D,E) depict the time histories at different tongues along the NNM 1 branch. The time response of point (C) clearly shows that the second linear modal coordinate (magenta line) had a large response amplitude at a frequency three times that of the first modal coordinate (black line), confirming the 3:1 interaction with NNM 2. As the FEP followed the α-tongue, the contribution of the second modal coordinate grew, but eventually returned to a lower amplitude as the tongue came back to the backbone (even though the second modal coordinate still contributed to the response along the backbone). The same observations were made with the other tongues and modal interactions, where the modal coordinate of the interacting mode oscillated at a higher harmonic than the first modal coordinate, i.e., 9:1 and 15:1 interactions in Figs. 3(D,E), respectively.

Once the NNMs have been computed, Eq. (15) was used to estimate the monoharmonic driving force required to excite the NNM motion. A mass and stiffness proportional damping model was used, defining the damping matrix as $\mathbf{C} = a\mathbf{K}+b\mathbf{M}$ with $a = -0.0391$ and $b = 1.47\,10^{-4}$. These parameters were chosen such that the damping ratios of the first and second linear modes were 1% and 5%, respectively. The computed force amplitude and the corresponding frequency are displayed for the first NNM in Fig. 4(b); the NNM is repeated in Fig. 4(a). Interestingly, the force does not increase monotonically. For example, a force of 22.6 N could achieve resonance at about 37.5 Hz, 45.8 Hz and 47.4 Hz as shown with the circular markers. This has important implications for the forced response, as will be discussed in the next section.

4 Numerical Case Study: Nonlinear Forced Response of a Cantilever Beam

4.1 Response to Sine Sweep Excitation

Some unexpected behavior occurred with the damped beam, using the same damping model described in the previous section, when a single-point force was applied 0.21 m from the fixed end in the transverse direction. A set of numerically computed sine sweeps are shown in Fig. 5, which plots the displacement of the beam tip for different force

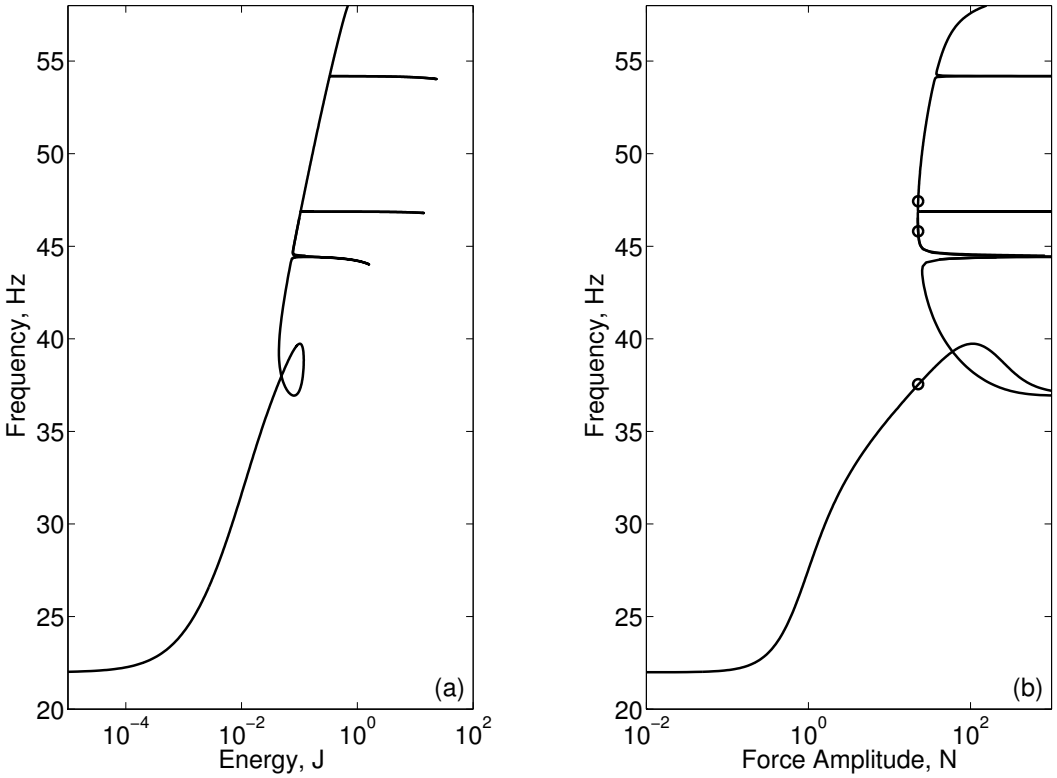

Figure 4: First NNM: (a) FEP, (b) estimate of force amplitude required to obtain the motion given at each point on NNM 1 when the input is at 0.21 m from the fixed end, as predicted by Eq. (15). Circular markers indicate achievable resonance frequencies for a force of 22.6 N.

amplitudes, namely $A = 11.3$ N, 22.6 N, 26.7 N, 32.5 N, 35.6 N, and 45.2 N, with a sweep rate of 0.5 Hz/s. For reference, the response of the linear model at a force amplitude of $A = 4.45$ N was computed (black line), and resulted in the largest tip displacement (even though the force amplitude was lowest), with a resonance at the linear natural frequency. The nonlinear spring caused the tip to displace at a significantly lower amplitude, and shifted the resonant frequency depending on the force amplitude. The nonlinear sweep at the force amplitude $A = 11.3$ N (red line) showed that resonance occurred near 37 Hz, resulting in a sudden jump, the so-called jump phenomenon, to a lower response amplitude as the frequency continued to sweep upwards. When the force amplitude doubled (green line, $A = 22.6$ N), the resonant frequency occurred near 39 Hz. However, doubling the force amplitude once more (cyan line, $A = 45.2$ N) caused a dramatic shift in resonant frequency and tip displacement. Now the response dropped off around 57 Hz, indicating that the increased force amplitude from 22.6 N to 45.2 N shifted the resonance nearly 18 Hz. Considering the amplitudes $A = 32.5$ N and 35.6 N (yellow and magenta lines) shows that the dramatic shift in resonant frequency occurred in this range of forcing amplitudes. Summarizing, Figure 5 depicts that *both a jump in amplitude (the well-known jump phenomenon) and a jump in frequency may exist for nonlinear systems.* We

could not find other occurrences of simultaneous jumps in amplitude and frequency in the mechanical engineering literature.

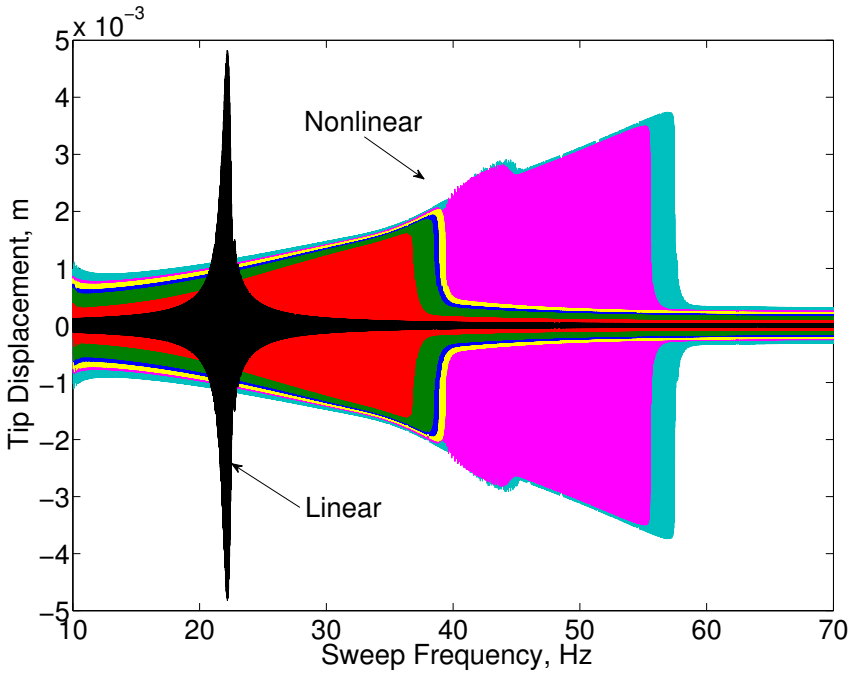

Figure 5: Numerical sine sweeps at a rate of 0.5 Hz/s where the displacement of the beam tip is plotted for force amplitudes of (red) 11.3 N, (green) 22.6 N, (blue) 26.7 N, (yellow) 32.5 N, (magenta) 35.6 N and (cyan) 45.2 N.

Another dynamical phenomenon, which only appeared for $A = 35.6$ N and 45.2 N, is the modulation of the signal's envelope in the range of 40-45 Hz. It was further examined by monitoring fold and Neimark-Sacker bifurcations [48] along the NLFR. Figure 6 superposes the sine sweep and NLFR responses for $A = 45.2$ N. Around 40 Hz, a Neimark-Sacker bifurcation changes the stability of the NLFR and generates a new branch of quasiperiodic oscillations (not shown in the figure). As a result, a stable torus attracts the dynamics and is responsible for the observed envelope modulation. Around 45 Hz, a second Neimark-Sacker bifurcation transforms the quasiperiodic motion back into stable periodic motion. There is a small delay between the first (second) bifurcation and the onset (disappearance) of quasiperiodic motion; this delay can be attributed to the transient character of the swept-sine excitation. At 56.6 Hz, a fold bifurcation occurs in the vicinity of resonance. The periodic solutions become unstable until a second fold bifurcation occurs around 38 Hz and the solutions become stable again. As a result of these bifurcations, the NLFR curves show a range of frequencies where multiple steady state solutions coexist for a fixed input frequency and amplitude. These coexisting periodic orbits make the forced response strongly dependent on the initial conditions of the system.

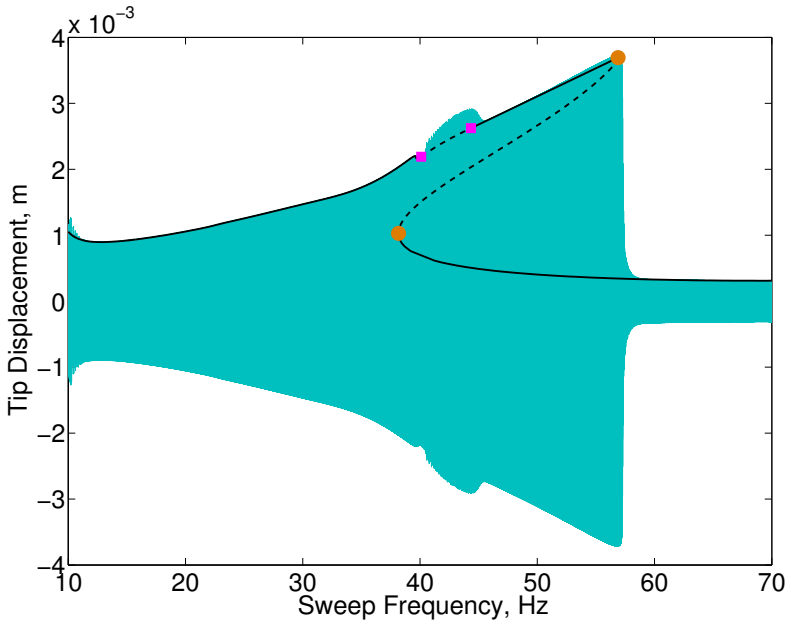

Figure 6: Beam displacement at tip. Response to a swept- and a stepped-sine (numerical continuation) excitation of 45.2 N depicted in cyan and black, respectively. Solid- and dashed-black lines denote stable and unstable periodic solutions, respectively. Fold and Neimark-Sacker bifurcations are pictured with orange bullets (●) and magenta squares (■), respectively.

4.2 Response to Stepped Sine Excitation

An explanation for the jump in frequency of Fig. 5 was sought by computing the NLFR through a range of frequencies that spanned the first NNM. A single-point, monoharmonic force with arbitrary complex amplitude $A+i0$ was applied to the beam at the same location as the sweeps. The FEPs of the forced response at four different forcing amplitudes (A = 0.445 N, 0.890 N, 2.22 N and 4.45 N) are shown in the left plot of Fig. 7, where the energy on the horizontal axis represents the maximum energy of each steady-state solution in the NLFR, and the vertical axis represents the forcing frequency. The NNM was superposed on the plot to show how the forced response wraps around the NNM, acting as the backbone to the NLFR.

As the forcing frequency increased from 20 Hz, a fold bifurcation occurred in the NLFR and turned back around the backbone of the NNM. At this fold, the MIF from Eq. (11) in the right plot in Fig. 7 is approximately equal to 1 indicating that the NLFR approximately excited the NNM motion of the underlying undamped system.

Higher forcing amplitudes (A = 11.3 N, 22.6 N, 26.7 N, 35.6 N, and 45.2 N) were considered in Fig. 8 in order to examine the response near the α-tongue on NNM 1 and to match some of the amplitudes used in the sine sweep results. For A = 11.3 N in Fig. 8(a), the NLFR again wrapped around the backbone of the first NNM, as previously observed in Fig. 7. When the force amplitude doubled (A = 22.6 N in Fig. 8(b)), the resonance on

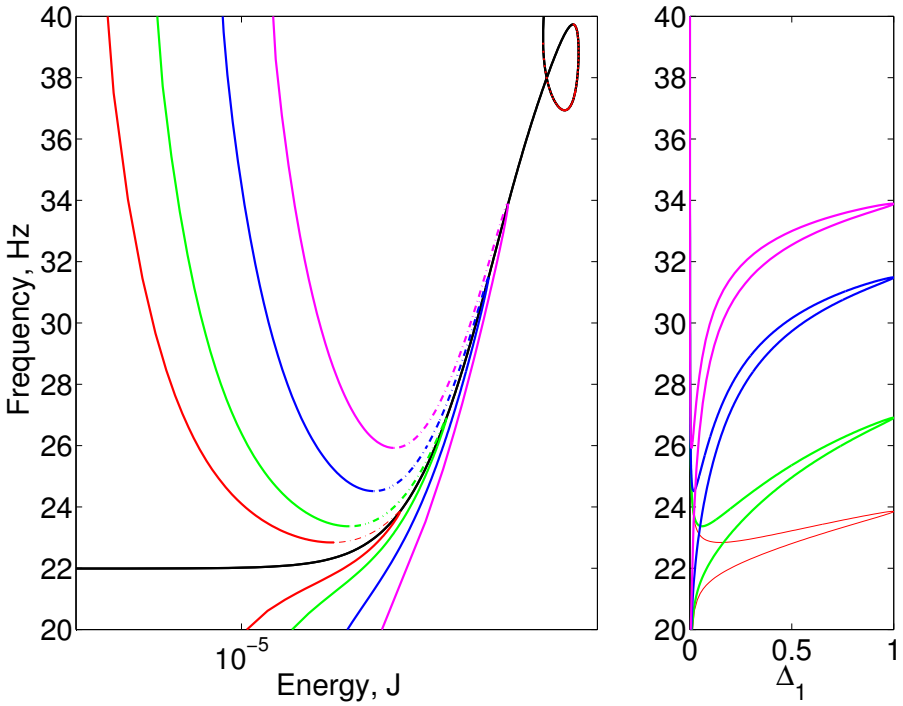

Figure 7: (Left) Nonlinear forced response curves at frequencies near the first NNM where (solid) are stable periodic motions and (dash dot) are unstable periodic motions. (Right) Mode indicator function of the forced response. The force amplitudes for each curve are (red) 0.445 N, (green) 0.890 N, (blue) 2.22 N, and (magenta) 4.45 N.

the main NLFR branch occurred at 38.1 Hz and approached the 3:1 modal interaction on NNM 1. Initially, the green curve on the left is all that was computed by the continuation algorithm, since it started at low frequency and followed the curve upwards. However, the force estimated in Fig. 4(b) suggested that resonance might be excited at multiple points on the NNM using the same force. Specifically, this figure highlighted that a force of 22.6 N could achieve resonance at about 37.5 Hz, 45.8 Hz and 47.4 Hz. So the two latter points were used to initiate the NLFR algorithm and obtain the branch between 43 and 48 Hz in Fig. 8(b). This additional branch is referred to as an isolated resonance curve, or IRC. The response on this IRC is much larger than on the main branch so one would significantly underestimate the response if it was not found. By examining the NNMs and employing the energy balance criterion introduced in Sec. 2.4 we have avoided dramatically under-predicting the resonant response at this forcing amplitude. These new solutions still wrapped around the backbone of NNM 1 and corresponded to the NNM at two different frequencies, 43.9 Hz and 48.5 Hz, as indicated by the MIF. These frequencies are in relatively close agreement with the frequencies predicted using the energy balance criterion, 45.8 Hz and 47.4 Hz.

The forcing amplitude was slightly increased in Fig. 8(c) ($A = 26.7$ N), and the resonant frequency on the main branch did not shift very much (from 38.1 Hz to 38.5 Hz). The fold bifurcation on the main NLFR branch still transpired prior to the modal interaction on NNM 1. Again the IRC persisted and became larger, increasing its frequency range

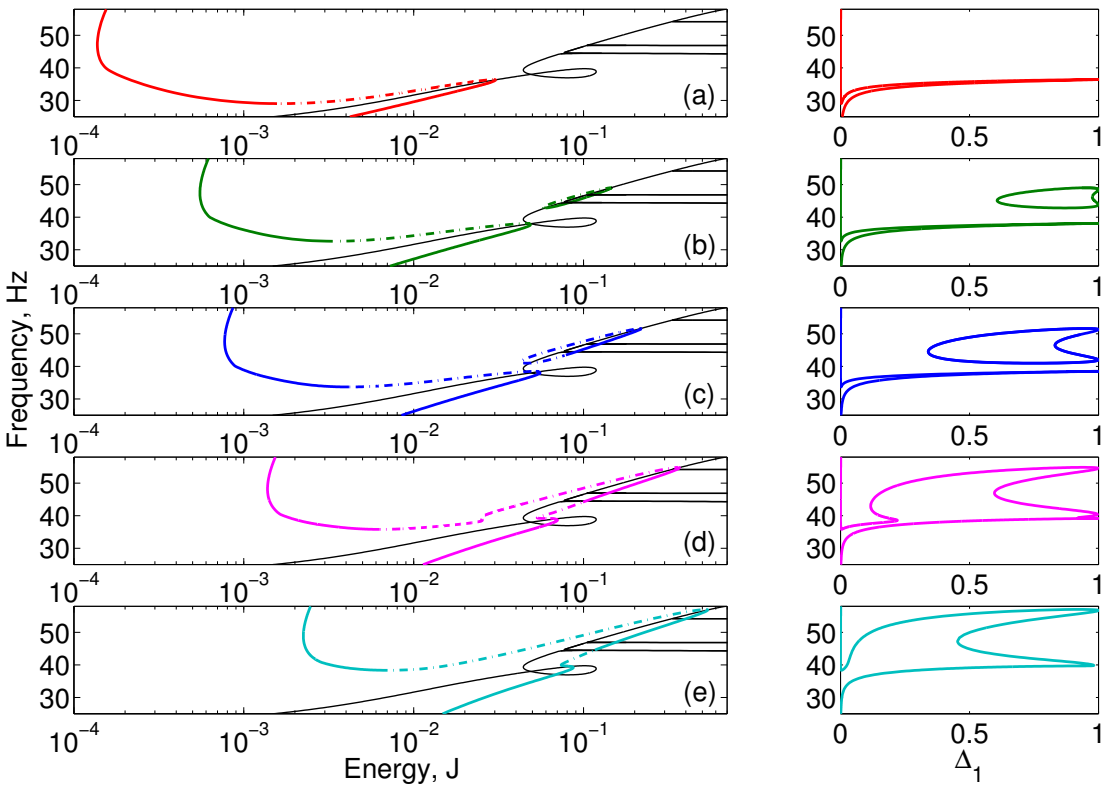

Figure 8: (Left) Nonlinear forced response curves at frequencies near the first NNM where (solid) are stable periodic motions and (dash dot) are unstable periodic motions. (Right) Mode indicator function of the forced response.The force amplitudes for each curve (a - e) are (red) 11.3 N, (green) 22.6 N, (blue) 26.7 N, (magenta) 35.6 N, and (cyan) 45.2 N, respectively.

from 41 Hz to 51 Hz. A stable portion of the IRC has however become unstable through the emergence of Neimark-Sacker bifurcations (not represented). The latter will persist at higher forcing levels and are responsible for the quasiperiodic oscillations discussed in Fig. 6.

Increasing the amplitude even more ($A = 35.6$ N in Fig. 8(d)) caused the main branch and the IRC to merge together, forming one continuous NLFR branch up to 55 Hz. The merging of these two branches offers an explanation as to why the jump in resonant frequency occurred during the sine sweep excitation in Fig. 5. The sine sweeps at $A = 22.6$ N, $A = 26.7$ N and $A = 32.5$ N fell off around 38 Hz, because the IRC was disconnected from the main branch, and there was no path for the response to follow to the higher frequency resonance. However, once the two NLFR branches merged together (A=35.6 N), the sine sweeps were able to stay along the high amplitude path up to resonance around 55 Hz.

For the highest forcing amplitude shown ($A = 45.2$ N in Fig. 8(e)), the resonant frequency shifted to 56.6 Hz. This smooth increase in the resonant frequency and displacement amplitude continued at higher forces as well. Moving from Fig. 8(d) to Fig. 8(e) also caused one resonance to be eliminated, as indicated by the MIF.

The FEPs of the NNM and NLFR effectively condense the complicated dynamics of the nonlinear beam onto a two-dimensional plane, however additional insight can be gained by looking at the time histories of the response, particularly when the MIF indicated a resonance on the NLFR. Figure 9 shows the time histories of the three resonant solutions (represented by circle markers) along the NLFR curves with forcing amplitude $A = 26.7$ N together with the time histories of the NNM near them. The periodic response was again projected onto the linear modal coordinates. The first linear modal coordinate dominated all three of the resonant responses, and the second mode contributed significantly as well, and its response clearly included higher order harmonics. The comparison between the NLFR and the corresponding NNM all were in good agreement, especially for the first modal coordinate. There was slight phase shift however for solution (a) when looking at the response of the second modal coordinate. This can be explained by the use of a monoharmonic force input, whereas a multi-harmonic force would be needed to exactly isolate the NNM.

4.3 Energy Balance Criterion

For further validation of the energy balance criterion (15), Figure 10 superposes the responses of Figs. 7 and 8 where the MIF is equal to 1 onto Fig. 4(b). The cross markers, which represent the forced resonant response, are in close, though not exact, agreement with the predictions of the energy balance criterion.

Additional insight can be gained from this plot. For instance, one can guess from the leftmost point of the upper branch the amplitude and frequency at which the IRC is created, i.e., 22.3 N and 46.5 Hz. Considering that the IRC merges with the main branch around 35 N, the jump in frequency can be predicted by considering the point at 35 N on

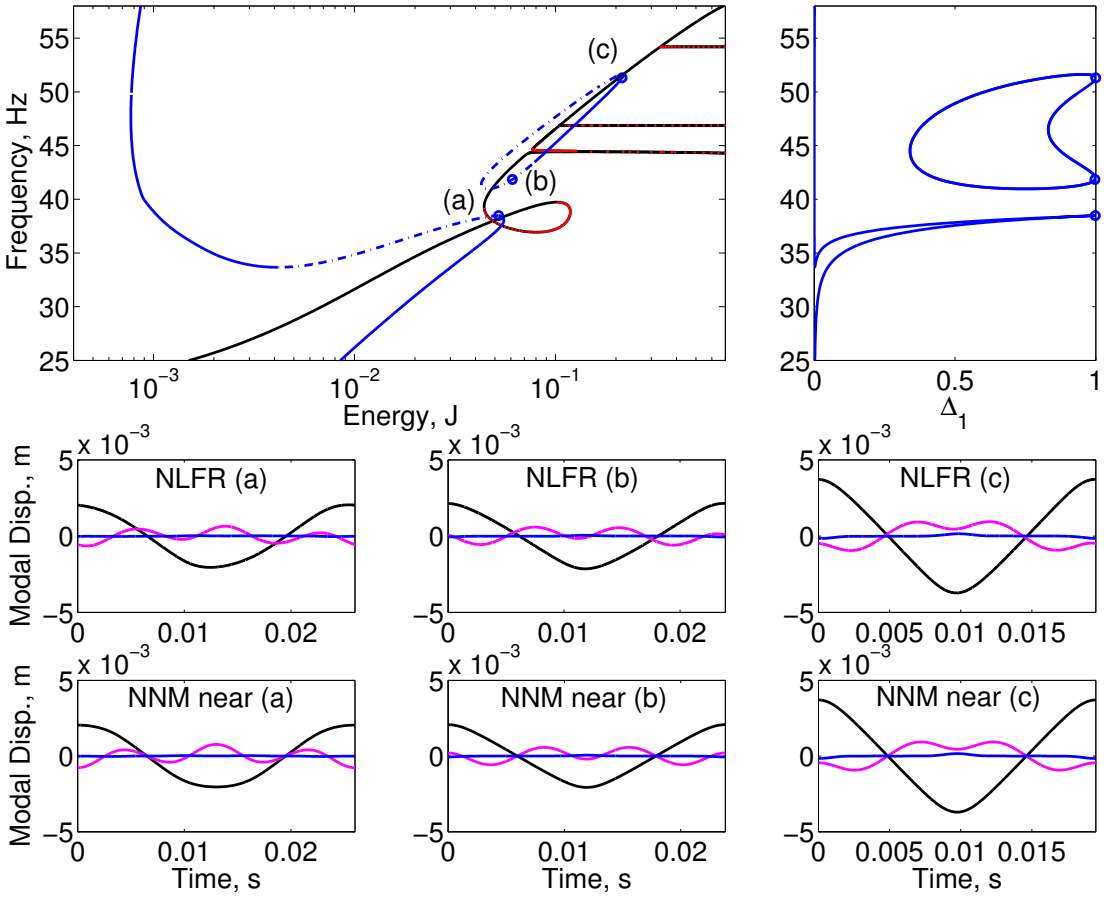

Figure 9: Comparing the time histories of the response projected onto unit displacement normalized modal coordinates at the three resonant conditions of the NLFR at force amplitude $A = 26.7$ N. The color code for the time response is (black) mode 1, (magenta) mode 2 and (blue) mode 3.

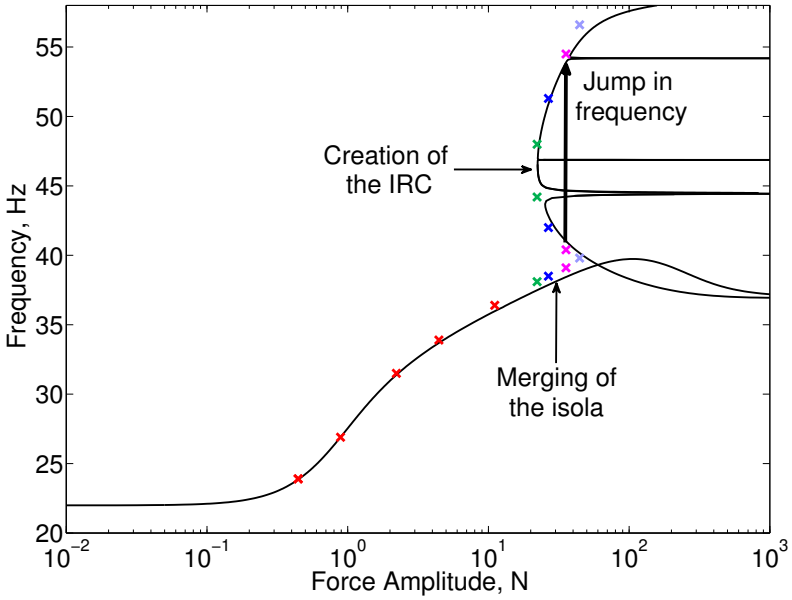

Figure 10: Comparison between the predictions of the energy balance criterion (solid black) and the forced resonance where the MIF is equal to one in Figs. 7 and 8 (cross markers).

the upper branch at 53.8 Hz.

Finally, one important observation about the birth and the merging of the IRC was that they occurred when the main NLFR branch approached the 3:1 interaction between NNM 1 and NNM 2. Indeed, this interaction produced the non-monotonic increase in the forcing amplitude observed in Fig. 4(b), which was found to be the driving mechanism for IRC onset in Section 4.2. This demonstrates that interactions between NNMs are responsible for the IRCs in the forced response. It should be noted that this behavior was not found to occur with other modal interactions on the NNM branch whose tongues were sharper in the FEP. We also stress that the NNM definition relies on the underlying Hamiltonian system, whereas the NLFR is a result for the damped system. Damping also plays a role in the existence of IRCs, that is they may cease to exist if damping is large enough. This is illustrated in the next section.

5 Fold Bifurcation Tracking and Influence of Damping

Bifurcation tracking in the codimension-2 space (frequency-forcing amplitude-energy) was performed in order analyze the evolution of the fold bifurcations for different forcing amplitudes. The procedure used in this section is based on the harmonic balance method described in [49], which approximates the periodic solutions with Fourier series (truncated

to the first seven harmonics herein). The 3D bifurcation locus is presented as an orange line in Fig. 11(a), which also shows the NLFR in black for forcing amplitudes of 25 N, 33.1 N and 40 N. Figure 11(b) gives a convenient projection of the bifurcation branch onto the frequency versus forcing amplitude plane. The turning point indicated with a diamond marker shows the frequency/forcing amplitude at which the fold bifurcations at the tips of the IRC were created. The corresponding values (45.7 Hz and 20.7 N) reflect the good predictive capability of the energy balance criterion (46.5 Hz and 22.3 N in Section 4.3). The square marker indicates when the IRC merges with the main resonance peak (33.1 N).

The fold bifurcation tracking analysis was again used to study the effect of structural damping on the observed IRCs. The damping matrix introduced in Section 4 was perturbed by adding a scaling term, κ, such that $\mathbf{C} = \kappa\,(-0.0391\mathbf{K} + 1.47\,10^{-4}\mathbf{M})$. Several bifurcation branches are given in Fig. 12 for different values of κ, namely 1, 1.5, 1.8 and 1.9. The IRC was robust against damping since it was still visible for higher levels of damping ($\kappa > 1$), however, increasing κ caused the IRC to appear later in forcing amplitude, and shorten the range where it existed. For the largest damping case studied, for $\kappa = 1.9$, the IRC was no longer present. This analysis shows that a sufficiently large value of structural damping can destroy the IRCs.

6 Conclusion

This paper demonstrates the intimate connection that exists between nonlinear normal modes (NNMs), i.e., the periodic motions of the undamped, unforced system, and the forced response of the damped system. To bridge the gap between these two types of response, the energy balance criterion was adapted so it could be used with the results of the numerical computations in order to estimate the resonant response to harmonic forcing from the NNMs and the damping matrix. This criterion strengthens the link that exists between NNMs and the resonant responses of the damped, forced system.

We have also shown that interactions between NNMs with non-necessarily commensurate linear frequencies are responsible for the isolated resonance curves (IRCs) in the forced response. IRCs, which might easily be missed during numerical continuation or experimental testing, have important practical consequences. The associated response can be much larger than on the main branch, and, when they connect to the main resonance branch, they may lead to a dramatic jump in frequency. To the best of our knowledge, this is the first time that this jump in frequency is observed in the mechanical engineering literature.

Finally, these developments extend the usefulness of the NNM concept to the interpretation of the complex dynamics exhibited by harmonically forced nonlinear systems.

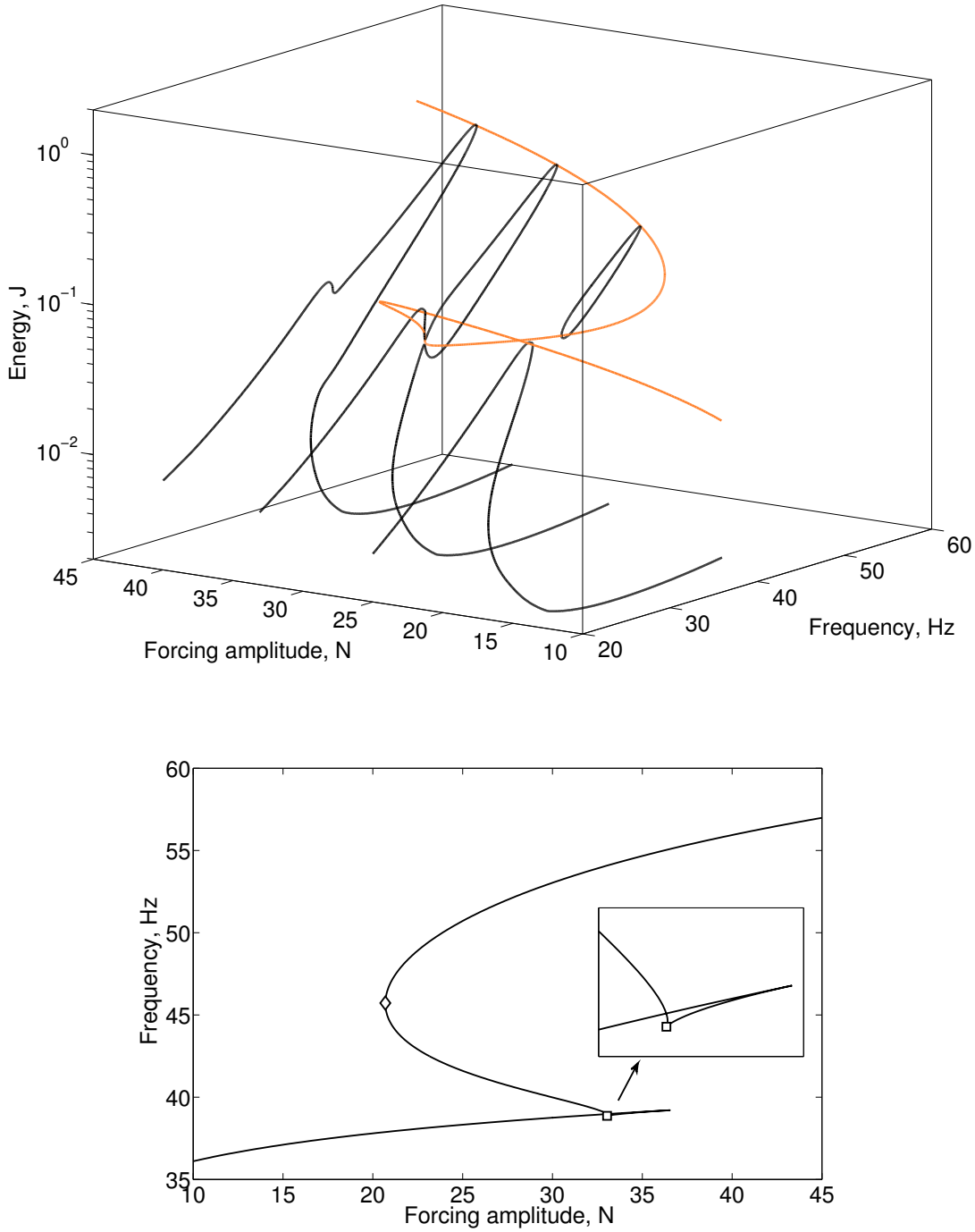

Figure 11: (a) Tracking of fold bifurcations. The black lines denote nonlinear forced response curves at forcing amplitudes of 25 N, 33.1 N and 40 N, and the orange line represent the locus of fold bifurcations. (b) Projection of the bifurcation branch onto the (forcing amplitude - energy) plane. The diamond and square markers indicate the apparition and the merging of the IRC, respectively.

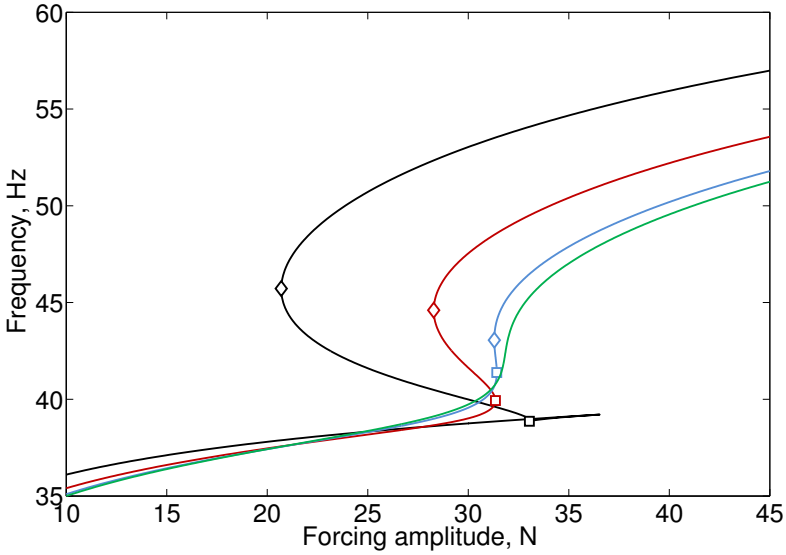

Figure 12: Influence of damping on the bifurcation branches. The black, red, blue and green lines depict the branches of the system with $\kappa = 1$, 1.5, 1.8 and 1.9, respectively. The diamond and square markers indicate the apparition and the merging of the IRC, respectively.

Acknowledgments

The author RJ Kuether would like to acknowledge the funding for this part of this research from the National Physical Science Consortium (NPSC) Fellowship. The author L. Renson is Research Fellow (FRIA fellowship) of the *Fonds de la Recherche Scientifique - FNRS*, which is gratefully acknowledged. The authors T. Detroux, C. Grappasonni and G. Kerschen would like to acknowledge the financial support of the European Union (ERC Starting Grant NOVIB 307265).

References

[1] D.J. Segalman, D.L. Gregory, M.J. Starr, B.R. Resor, M.D. Jew, J.P. Lauffer, and N.M. Ames, *Handbook on Dynamics of Jointed Structures*, Sandia National Laboratories, Albuquerque, NM2009.

[2] D.A. Czaplewski, C.W. Dyck, H. Sumali, J.E. Massad, J.D. Kuppers, I. Reines, W.D. Cowan, and C.P. Tigges, A Soft Landing Waveform for Actuation of a Single Pole Single Throw Ohmic RF MEMS Switch, *Journal of Micromech. Sys.*, vol. 15, pp. 1586-94, 2006.

[3] M. Garcia, A. Chatterjee, A. Rulna, and M. Coleman, The Simplest Walking model: Stability, Complexity, and Scaling, *Transactions of the ASME. Journal of Biomechanical Engineering*, vol. 120, pp. 281-8, 1998.

[4] O. Gendelman, Bifurcations of Nonlinear Normal Modes of Linear Oscillator with Strongly Nonlinear Damped Attachment, *Nonlinear Dynamics*, vol. 37, pp. 115-128, 2004.

[5] A.F. Vakakis, D.M. McFarland, L. Bergman, L.I. Manevitch, and O. Gendelman, Isolated Resonance Captures and Resonance Capture Cascades Leading to Single- or Multi-Mode Passive Energy Pumping in Damped Coupled Oscillators, *Journal of Vibration and Acoustics*, vol. 126, pp. 235-244, 2004.

[6] D.J. Segalman, M.R. Brake, L.A. Bergman, A.F. Vakakis, and K. Willner, Epistemic and Aleatoric Uncertainty in Modeling, *Proceedings of the ASME 2013 International Design Engineering Technical Conferences IDETC*, Portland, Oregon, 2013.

[7] R. M. Rosenberg, Normal modes of Nonlinear Dual-Mode Systems, *Journal of Applied Mechanics*, vol. 27, pp. 263âĂŞ268, 1960.

[8] S.W. Shaw, and C. Pierre, Normal Modes for Non-Linear Vibratory Systems, *Journal of Sound and Vibration*, vol. 164, pp. 85-124, 1993.

[9] A.F. Vakakis, Non-linear Normal Modes (NNMs) and their Applications in Vibration Theory: an Overview, *Mechanical Systems and Signal Processing*, vol. 11, pp. 3-22, 1997.

[10] A.F. Vakakis, L.I. Manevitch, Y.V. Mikhlin, V.N. Pilipchuk, and A.A. Zevin, *Nonlinear Modes and Localization in Nonlinear Systems*, New York, Wiley, 1996.

[11] G. Kerschen, M. Peeters, J.C. Golinval, and A.F. Vakakis, Nonlinear Normal Modes. Part I. A useful framework for the structural dynamicist, *Mechanical Systems and Signal Processing*, vol. 23, pp. 170-94, 2009.

[12] W. Lacarbonara, R. Camillacci, Nonlinear Normal Modes of Structural Systems via Asymptotic Approach, *International Journal of Solids and Structures*, vol. 41, pp. 5565-5594, 2004.

[13] C. Touzé and M. Amabili, Nonlinear Normal Modes for Damped Geometrically Nonlinear Systems: Application to Reduced-Order Modelling of Harmonically Forced Structures, Journal of Sound and Vibration, vol. 298, pp. 958-981, 2006.

[14] R. Arquier, S. Bellizzi, R. Bouc, and B. Cochelin, Two Methods for the Computation of Nonlinear Modes of Vibrating Systems at Large Amplitudes, *Computers & Structures*, vol. 84, pp. 1565-1576, 2006.

[15] R.J. Kuether and M.S. Allen, A Numerical Approach to Directly Compute Nonlinear Normal Modes of Geometrically Nonlinear Finite Element Models, *Mechanical Systems and Signal Processing*, vol. 46, pp. 1-15, 2014.

[16] D. Laxalde and F. Thouverez, Complex Non-linear Modal Analysis for Mechanical Systems: Application to Turbomachinery Bladings with Friction Interfaces, *Journal of Sound and Vibration*, vol. 322, pp. 1009-1025, 2009.

[17] M. Peeters, R. Viguié, G. Sérandour, G. Kerschen, and J. C. Golinval, Nonlinear Normal Modes, Part II: Toward a Practical Computation using Numerical Continuation Techniques, *Mechanical Systems and Signal Processing*, vol. 23, pp. 195-216, 2009.

[18] E. Pesheck, C. Pierre, and S.W. Shaw, New Galerkin-based Approach for Accurate Non-linear Normal Modes through Invariant Manifolds, *Journal of Sound and Vibration*, vol. 249, pp. 971-993, 2002.

[19] L. Renson, G. Deliége, and G. Kerschen, An Effective Finite-Element-Based Method for the Computation of Nonlinear Normal Modes of Nonconservative Systems, *Meccanica*, vol. 49, pp. 1901-1916, 2014.

[20] G. Kerschen, M. Peeters, J.C. Golinval, and C. Stephan, Nonlinear Normal Modes of a Full-Scale Aircraft, *AIAA Journal of Aircraft*, vol. 50, pp. 1409-1419, 2013.

[21] M. Krack, L. Panning-von Scheidt, and J. Wallaschek, A Method for Nonlinear Modal Analysis and Synthesis: Application to Harmonically Forced and Self-Excited Mechanical Systems, *Journal of Sound and Vibration*, vol. 332, pp. 6798-6814, 2013.

[22] L. Renson, J.P. Noel, and G. Kerschen, Complex Dynamics of a Nonlinear Aerospace Structure: Numerical Continuation and Normal Modes, *Nonlinear Dynamics*, in press.

[23] M. Peeters, G. Kerschen, and J.C. Golinval, Dynamic Testing of Nonlinear Vibrating Structures using Nonlinear Normal Modes, *Journal of Sound and Vibration*, vol. 330, pp. 486-509, 2011.

[24] M. Peeters, G. Kerschen, and J. C. Golinval, Modal Testing of Nonlinear Vibrating Structures based on Nonlinear Normal Modes: Experimental Demonstration, *Mechanical Systems and Signal Processing*, vol. 25, pp. 1227-1247, 2011.

[25] D. Ehrhardt, R. Harris, and M. Allen, Numerical and Experimental Determination of Nonlinear Normal Modes of a Circular Perforated Plate, in *Topics in Modal Analysis I*, Volume 7, J. De Clerck, Ed., ed: Springer International Publishing, 2014, pp. 239-251.

[26] J.L. Zapico-Valle, M. Garcia-Diéguez, and R. Alonso-Camblor, Nonlinear Modal Identification of a Steel Frame, *Engineering Structures*, vol. 56, pp. 246-259, 2013.

[27] A. Cammarano, T.L. Hill, S.A. Neild, D.J. Wagg, Bifurcations of Backbone Curves for Systems of Coupled Nonlinear Two Mass Oscillator, *Nonlinear Dynamics*, vol. 77, 311-320.

[28] A.H. Nayfeh, *Nonlinear Interactions*, Wiley, New York, 2000.

[29] M.R. Marsico, V. Tzanov, D.J. Wagg, S.A. Neild, B. Krausskopf, Bifurcation Analysis of a Parametrically Excited Inclined Cable Close to 2:1 Internal Resonance, *Journal of Sound and Vibration*, vol. 330, 6023-6035.

[30] N. Srinil, and G. Rega, 2:1 Resonant Multi-Modal Dynamics of Horizontal/Inclined Cables, Part II: Internal Resonance Activation, Reduced-Order Models and Nonlinear Normal Modes, *International Journal of Non-linear Mechanics*, vol. 42, 515-528, 2007.

[31] S. Dou, B.S. Strachan, S.W. Shaw, and J.S. Jensen, Characterization and Optimal Design of Nonlinear MEMS Resonators, *Sold-State Sensors, Actuators and Microsystems Workshop*, Hilton Head, 2014.

[32] T.L. Hill, P.L. Green, A. Cammarano and S.A. Neild, Fast Bayesian Identification of Multi-mode Systems using Backbone Curves, *Journal of Sound and Vibration*, in preparation.

[33] G. Gatti, M.J. Brennan, and I. Kovacic, On the Interaction of the Responses at the Resonance Frequencies of a Nonlinear Two Degrees-of-freedom System, *Physica D: Nonlinear Phenomena*, vol. 239, pp. 591-599, 2010.

[34] G. Gatti and M.J. Brennan, On the Effects of System Parameters on the Response of a Harmonically Excited System Consisting of Weakly Coupled Nonlinear and Linear Oscillators, *Journal of Sound and Vibration*, vol. 330, pp. 4538-4550, 2011.

[35] N.A. Alexander and F. Schilder, Exploring the Performance of a Nonlinear Tuned Mass Damper, *Journal of Sound and Vibration*, vol. 319, pp. 445-462, 2009.

[36] C. Duan and R. Singh, Isolated Sub-Harmonic Resonance Branch in the Frequency Response of an Oscillator with Slight Asymmetry in the Clearance, *Journal of Sound and Vibration*, vol. 314, pp. 12-18, 2008.

[37] T.L. Hill, A. Cammarano, S.A. Neild and D.J. Wagg, An Analytical Method for the Optimisation of Weakly Nonlinear Systems, *Proceedings of the 9th International Conference on Structural Dynamics - EURODYN 2014*, Porto, Portugal, 2014.

[38] T.L. Hill, A. Cammarano, S.A. Neild and D.J. Wagg, Interpreting the Forced Response of a Two-Degree-Of-Freedom Nonlinear Oscillator using Backbone Curves, *Submitted to Journal of Sound and Vibration*, 2014.

[39] D.J. Segalman, A Four-Parameter Iwan Model for Lap-Type Joints, *Journal of Applied Mechanics*, vol. 72, pp. 752-760, 2005.

[40] Y.S. Lee, G. Kerschen, A.F. Vakakis, P. Panagopoulos, L.A. Bergman, D.M. McFarland, Complicated Dynamics of a Linear Oscillator with an Essentially Nonlinear Local Attachment, *Physica D*, vol. 204, pp. 41-69, 2005.

[41] B. Cochelin and C. Vergez, A High Order Purely Frequency-Based Harmonic Balance Formulation for Continuation of Periodic Solutions, *Journal of Sound and Vibration*, vol. 324, pp. 243-262, 2009.

[42] S.M. Roberts and J.S. Shipman, *Two-Point Boundary Value Problems: Shooting Methods*, New York, American Elsevier, 1972.

[43] O. Tanrikulu, B. Kuran, H.N. Ozguven, and M. Imregun, Forced Harmonic Response Analysis of Nonlinear Structures using Describing Functions, *AIAA Journal*, vol. 31, pp. 1313-1320, 1993.

[44] E.P. Petrov and D.J. Ewins, Analytical Formulation of Friction Interface Elements for Analysis of Nonlinear Multi-Harmonic Vibrations of Bladed Disks, *Journal of Turbomachinery*, vol. 125, pp. 364-371, 2003.

[45] M.W. Sracic and M.S. Allen, Numerical Continuation of Periodic Orbits for Harmonically Forced Nonlinear Systems, *Proceedings of the 29th International Modal Analysis Conference (IMAC XXIX)*, Jacksonville, Florida, 2011.

[46] R.J. Kuether and M.S. Allen, Computing Nonlinear Normal Modes using Numerical Continuation and Force Appropriation, *Proceedings of the ASME 2012 International Design Engineering Technical Conferences IDETC/CIE*, Chicago, Illinois, 2012.

[47] M. Geradin, D. Rixen, *Mechanical Vibrations; Theory and Application to Structural Dynamics*, Wiley, 1997.

[48] A.V. Kuznetsov, *Elements of Applied Bifurcation Theory*, Springer, New York, 2004.

[49] T. Detroux, L. Renson, and G. Kerschen, The Harmonic Balance Method for Advanced Analysis and Design of Nonlinear Mechanical Systems. In G. Kerschen, Ed., *Nonlinear Dynamics*, Volume 2, pp. 19-34, Springer International Publishing, 2014.